

Three-body correlations in direct reactions: Example of ${}^6\text{Be}$ populated in (p, n) reaction

V. Chudoba,^{1,2,*} L.V. Grigorenko,^{1,3,4} A.S. Fomichev,¹ A.A. Bezbakh,¹ I.A. Egorova,^{5,6} S.N. Ershov,⁵ M.S. Golovkov,¹ A.V. Gorshkov,¹ V.A. Gorshkov,¹ G. Kaminski,^{1,7} S.A. Krupko,¹ I. Mukha,⁸ E.Yu. Nikolskii,^{4,1} Yu.L. Parfenova,¹ S.I. Sidorchuk,¹ P.G. Sharov,¹ R.S. Slepnev,¹ L. Standylo,^{1,9} S.V. Stepantsov,¹ G.M. Ter-Akopian,¹ R. Wolski,^{1,10} and M.V. Zhukov¹¹

¹*Flerov Laboratory of Nuclear Reactions, JINR, 141980 Dubna, Russia*

²*Institute of Physics, Silesian University in Opava, 74601 Opava, Czech Republic*

³*National Research Nuclear University “MEPhI”, 115409 Moscow, Russia*

⁴*National Research Centre “Kurchatov Institute”, Kurchatov sq. 1, 123182 Moscow, Russia*

⁵*Bogoliubov Laboratory of Theoretical Physics, JINR, 141980 Dubna, Russia*

⁶*Department of Physics, Western Michigan University, Kalamazoo, MI 49008, USA*

⁷*Heavy Ion Laboratory, University of Warsaw, 02-093 Warszawa, Poland*

⁸*GSI Helmholtzzentrum für Schwerionenforschung, 64291 Darmstadt, Germany*

⁹*Heavy Ion Laboratory, University of Warsaw, Pasteura 5A, Warsaw, Poland*

¹⁰*Institute of Nuclear Physics PAN, Radzikowskiego 152, 31342 Kraków, Poland*

¹¹*Department of Physics, Chalmers University of Technology, S-41296 Göteborg, Sweden*

(Dated: January 21, 2022. d:/latex/6be-s3/6be-s3-5.tex)

The ${}^6\text{Be}$ continuum states were populated in the charge-exchange reaction ${}^1\text{H}({}^6\text{Li}, {}^6\text{Be})n$ collecting very high statistics data ($\sim 5 \times 10^6$ events) on the three-body $\alpha+p+p$ correlations. The ${}^6\text{Be}$ excitation energy region below ~ 3 MeV is considered, where the data are dominated by contributions from the 0^+ and 2^+ states. It is demonstrated how the high-statistics few-body correlation data can be used to extract detailed information on the reaction mechanism. Such a derivation is based on the fact that highly spin-aligned states are typically populated in the direct reactions.

I. INTRODUCTION

The nuclear driplines are defined by instability with respect to particle emission, and therefore the entire spectra of the systems beyond the driplines are continuous. The first emission threshold in the light even systems is often, due to pairing interaction, the threshold for two-neutron or two-proton emission, and therefore one has to deal with three-body continuum. In certain systems, just beyond the dripline, the continuum of more fragments in the final state can be encountered (e.g. ${}^7\text{H}$, ${}^8\text{C}$, ${}^{28}\text{O}$), so we should speak about few-body continuum. Few-body continuum provides rich information about nuclear structure of ground state and continuum excitations, which is, however, often tightly intertwined with contributions of reaction mechanism. The way to extract this information is to explore the world of various correlations in fragment motions and to look for methods to disentangle contributions of a reaction mechanisms.

Nuclear reactions provide much broader opportunities to study correlations in comparison with nuclear decays. Any reaction has at least one selected direction — the direction of a projectile momentum — and correlations of the reaction products relative to this direction can be studied. This fact is the starting point for a wide-spread method of spin-parity (J^π) identification in the excitation spectrum: experimental angular distribution of the reaction products is compared to Born-type calculations.

Such angular distributions can be qualitatively described in terms of transferred momentum \mathbf{q} and transferred angular momentum ΔL by a simple analytical expression for differential cross-section

$$\frac{d\sigma_{\Delta L}}{d\Omega} \sim |j_{\Delta L}(qr_0)|^2, \quad (1)$$

where $j_{\Delta L}$ is spherical Bessel function and r_0 is some typical size of the “reaction volume”. In spite of quite qualitative character of the dependence Eq. (1), in some cases, it could be sufficient for complete J^π identification. Applications of such methods are limited by field of *direct reactions*, where the Born-type approximations are robust.

Alternative method of spin-parity identification can be used for a *narrower class of the direct reactions* populating *states in the continuum*. Namely, for direct reactions which can be well described by the pole mechanism [or single diagram with transfer of one species, see Fig. 1 (a)], where one-step reaction gives dominating contribution. Such a mechanism is widespread at intermediate (20 – 70 AMeV) and high (>70 AMeV) energies which are commonly used in the modern radioactive ion beam (RIB) research. It selects one exceptional direction in space defined by the vector of the transferred momentum \mathbf{q} . In the coordinate frame where Z axis is parallel to \mathbf{q} , only a zero projection $\Delta M = 0$ of the orbital angular momentum ΔL can be transferred.

$$\{[\Delta \mathbf{L} \times \mathbf{q}] \equiv 0, Z \parallel \mathbf{q}\} \rightarrow \Delta M = 0. \quad (2)$$

This assumption may be applied only to transfer of spinless particles. However, in many reaction scenarios

* chudoba@jinr.ru

the states with $J > 1/2$ are populated with high spin-alignment in the momentum transfer frame even in the case of nonzero spin transfer. For highly aligned states, *decaying via particle emission*, the angular distributions with respect to the axis $Z \parallel \mathbf{q}$ could have very distinctive shape, which can be used for spin-parity identification.

This method was broadly used for spin-parity identification of excited states decaying via emission of (mainly spinless) particles in the past [1, and Refs. therein]. During the last decade, such an approach was applied to exotic neutron- and proton-rich systems beyond the driplines in the experiments at the Flerov Laboratory of Nuclear Reactions at JINR (Dubna, Russia). For example, the interference patterns for broad overlapping states with different J^π were used for unambiguous spin-parity identification of low-lying ^9He continuous states decaying via $^8\text{He}+n$ channel [2]. Analogous method can be used for three-body systems, however in a technically much more complicated manner. The examples of such a J^π identification in three-body systems can be found for ^5H [3, 4] and for ^{10}He states [5].

The first results of the experiment studying the $\alpha+p+p$ correlations in decays of the ^6Be states populated in the (p, n) charge-exchange reaction were published in Ref. [6]. The paper was focused on the proof that the observed ^6Be excitation spectrum above ~ 3 MeV is dominated by the novel phenomenon – isovector breed of the soft dipole mode “built” on the ^6Li ground state (g.s.). In this work we consider the correlations in the decay of ^6Be states with excitation energy below ~ 3 MeV, where the data are dominated by the contributions of the known and well-understood 0^+ and 2^+ states of ^6Be . We pursue a sort of an opposite aim to Refs. [2–5]. We demonstrate that basing on the *known level scheme* it is possible to extract from the three-body correlations the *maximal possible* quantum mechanical information about reaction mechanism (e.g. the density-matrix parameters) thus paving the way to its in-depth theoretical studies.

Unit system $\hbar = c = 1$ is used in this work. The article is structured in the following way. First, kinematics notations are given for three-particle correlations detected in a reaction with four particles in final state (Section II). Then a description of the applied theoretical model is presented in Section III in detail. The experimental setup and conditions are given in Section IV. The data analysis is described in Section V, and the physics discussion and conclusions are in Sections VI and VII, respectively.

II. THREE-BODY CORRELATIONS

Let us consider three-body correlations obtained in the nuclear reaction $^6\text{Li} + p \rightarrow (p + p + \alpha) + n$. In general, the spin-averaged cross section for a collision $A + p \rightarrow k_1 + k_2 + k_3 + k_n$ of a projectile A and a proton target p , leading to the four fragments in the final state, can be

written in the following way

$$\sigma = \frac{(2\pi)^4}{v_i} \frac{1}{\hat{J}_A^2 \hat{J}_p^2} \sum \int d\mathbf{k}_1 d\mathbf{k}_2 d\mathbf{k}_3 d\mathbf{k}_n \times \delta(E_f - E_i) \delta(\mathbf{P}_f - \mathbf{P}_i) |T_{fi}|^2, \quad (3)$$

where $E_i = E_p + E_A$, $E_f = E_1 + E_2 + E_3 + E_n + Q$, $\mathbf{P}_i = \mathbf{k}_p + \mathbf{k}_A$, $\mathbf{P}_f = \mathbf{k}_1 + \mathbf{k}_2 + \mathbf{k}_3 + \mathbf{k}_n$ are the total energies and momenta of all particles before and after collisions, respectively. $Q = -3.70$ MeV is the separation energy of the nucleus A (the reaction Q -value is calculated in respect to the three-body threshold in the final state), E_j is a kinetic energy of particle j . The relative incident velocity is $v_i = k_i/\mu_i$, and $\mu_i = m_p m_A/(m_p + m_A)$ is the reduced mass of the nuclei before collision. Short-cut $\hat{J} = \sqrt{2J+1}$ is used in (3), and the summation is over spin projections of all particles before and after collision. In the $(p + A)$ center-of-mass (c.m.) coordinate frame $\mathbf{P}_i = 0$, $\mathbf{k}_A = -\mathbf{k}_p = \mathbf{k}$, $E_i = k^2/2\mu_i$. Our prime interest is in studies of nuclear systems consisted out of the three particles k_1 , k_2 and k_3 . Then, the fragment relative motion in three-body continuum can be described by two relative Jacobi momenta \mathbf{k}_x and \mathbf{k}_y and the c.m. momentum \mathbf{k}' of the three particles

$$\begin{aligned} \mathbf{k}_x &= \mu_x \left(\frac{\mathbf{k}_1}{m_1} - \frac{\mathbf{k}_2}{m_2} \right), & \mu_x &= \frac{m_1 m_2}{m_{12}} \\ \mathbf{k}_y &= \mu_y \left(\frac{\mathbf{k}_1 + \mathbf{k}_2}{m_{12}} - \frac{\mathbf{k}_3}{m_3} \right), & \mu_y &= \frac{m_{12} m_3}{m_{123}} \\ \mathbf{P}_f &= 0, & \mathbf{k}' &= \mathbf{k}_1 + \mathbf{k}_2 + \mathbf{k}_3 = -\mathbf{k}_4 \end{aligned} \quad (4)$$

where $m_{12} = (m_1 + m_2)$, $m_{123} = (m_1 + m_2 + m_3)$. For each three-body decay event, the Jacobi momenta \mathbf{k}_x and \mathbf{k}_y define the decay plane. The *internal correlations* of the fragments [shown by red color in Fig. 1 (c)] are defined within this plane while *external correlations* [blue colored in Fig. 1 (c)] defines orientation of this plane with respect to the reaction plane [green colored in Fig. 1 (c)], which is fixed by the initial \mathbf{k} and final \mathbf{k}' c.m. momenta.

Internal three-body correlations for the Jacobi momenta \mathbf{k}_x and \mathbf{k}_y are conveniently described by two parameters $\{\varepsilon, \theta_k\}$ in the following way:

$$\begin{aligned} \varepsilon &= E_x/E_T, & \cos(\theta_k) &= (\hat{\mathbf{k}}_x \cdot \hat{\mathbf{k}}_y) \\ E_T &= E_x + E_y = k_x^2/2\mu_x + k_y^2/2\mu_y. \end{aligned} \quad (5)$$

The three-body decay energy E_T fixes only a total phase volume accessible for the three fragments, and the fragment kinetic energies have continuous distributions within this volume. In addition, two relative orbital angular momenta l_x and l_y , corresponding to the \mathbf{k}_x and \mathbf{k}_y momenta, characterize their motion. Since in the ^6Be two fragments are identical protons, only two different distinguishable Jacobi coordinate systems exist. One, labeled “T”, corresponds to the case when particles 1 and 2 are protons with relative momentum \mathbf{k}_x , while particle 3 is the α -particle. In the second case, called “Y”, the relative momentum \mathbf{k}_x is defined by the proton with index

boundary conditions. To get $\Psi^{(-)}$ one has to solve equations of the Faddeev-Yakubovsky type, taking into account the complex nature of the constituents. An exact solution has not been feasible up to now, and therefore approximate methods are required. We make approximations at the level of the reaction mechanism but the three-body structure of the involved nuclei is treated in a consistent way.

At low excitation energies of the ${}^6\text{Be}$ nucleus, the relative velocities of the ${}^6\text{Be}$ fragments are small and are restricted kinematically by the E_T . It means that interactions between these fragments have to be taken into account. But if collision is relatively fast and a one-step processes are dominated, then a reasonable approximation for $\Psi^{(-)}$ is the following factorization

$$\langle \Psi_{M_{p1}, M_{p2}, M_n}^{(-)}(\mathbf{k}_x, \mathbf{k}_y, \mathbf{k}_f) | \simeq \langle \chi_{M_n}^{(-)}(\mathbf{k}_f), \Psi_{M_{p1}, M_{p2}}^{(-)}(\mathbf{k}_x, \mathbf{k}_y) |, \quad (7)$$

where $\Psi_{M_{p1}, M_{p2}}^{(-)}(\mathbf{k}_x, \mathbf{k}_y)$ is a continuum three-body wave function of the ${}^6\text{Be}$ system with excitation energy E_T . $\chi_{M_n}^{(-)}(\mathbf{k}_f)$ is a distorted wave describing relative motion between c.m. of the ${}^6\text{Be}$ and neutron, which depends on the respective relative coordinate between their center of mass.

If fragments are detected in coincidence, a number of various correlations can be obtained. The exclusive cross section

$$d^8\sigma/d\hat{\mathbf{k}}_f d\hat{\mathbf{k}}_x d\hat{\mathbf{k}}_y d\varepsilon dE_T,$$

contains the maximum possible information about the nuclear structure and reaction dynamics that can be extracted from a three-body breakup induced by the collision of two unpolarized nuclei (projectile and target). Exploration of this cross section is quite a challenge both experimentally (huge statistics is demanded) and theoretically, because it involves too many independent variables for transparent analysis. Integrating out some unobserved degrees of freedom brings us to less-exclusive (increasingly inclusive) cross sections. Any integration over a dynamical variable, within its full range of variation, washes out the correlations defined by this degree of freedom. Cross sections after integration become less and less informative, but are simultaneously more suitable for theoretical modeling. On the other hand, often not all the particles produced by reaction are measured by detectors. Depending on the geometry of experimental installation and the efficiency of particle registration, some fragments avoid the measurements. Thus, for a proper comparison of theoretical calculations with experimental data, the integration over some unobserved degrees of freedom should be done not within a full range of variation but taking into account response of the experimental setup. Practical way to perform this task is to use the Monte-Carlo simulation of the reaction events. This allows to make an additional simplification in theoretical treatment of the reaction dynamics, namely to substitute

the distorted wave $\chi_{M_n}^{(-)}(\mathbf{k}_f)$ by a plane wave. Then, the product of two plane waves in the transition matrix element (6) is reduced to the plane wave which depends on the transferred momentum \mathbf{q}

$$\chi_{M_n}^{(-)*}(\mathbf{k}_f) \chi_{M_p}(\mathbf{k}_i) \simeq \exp[-(\mathbf{q} \cdot \mathbf{R})] | 1/2, M_p \rangle \langle 1/2, M_n |.$$

Finally, we treat the motion between c.m. of colliding systems within the plane wave approximation (PWA) but the three-body decay dynamics is considered in a full complexity by taking into account all interactions between fragments. The disadvantage of such a treatment is that we can not calculate absolute contributions to cross sections from excitations with different values J^π . However, relative contributions from possible excitation modes leading to the excitation with the fixed value of J^π can be calculated. The absolute weights of different J^π excitations are restored by fitting to the experimental data. Hereby we remedy our simplified plane wave treatment of the reaction dynamics.

The Hyperspherical Harmonics (HH) method is used for calculations of the three-body continuum wave function. The $\alpha+p+p$ wave function (WF) of ${}^6\text{Be}$ with outgoing asymptotics with fixed total momentum J and its projection M is obtained from solution of the Schrödinger equation with the source term

$$(\hat{H}_3 - E_T) \Psi_3^{JM(+)} = \hat{\mathcal{O}} \Psi_{6\text{Li}}^{J'M'}, \quad (8)$$

$$\hat{H}_3 = \hat{T}_3 + V_{12}(\mathbf{r}_{12}) + V_{23}(\mathbf{r}_{23}) + V_{31}(\mathbf{r}_{31}).$$

The wave function $\Psi_3^{JM(+)}$ is linked with the wave function $\Psi_{M_{p1}, M_{p2}}^{(-)}(\mathbf{k}_x, \mathbf{k}_y)$ in Eq. (7) by the reversal of time which involves reversing the linear momenta (\mathbf{k}_x and \mathbf{k}_y) and direction of the spin rotation ($M_i \rightarrow -M_i$). The effective charge-exchange interaction between projectile and target nucleons with Gaussian formfactor is used

$$\hat{V}(r) = V_0 \left[c_{ivs} + c_{ivv} \left(\sigma^{(1)} \cdot \sigma^{(2)} \right) \right] \times \left(\tau^{(1)} \cdot \tau^{(2)} \right) \exp \left[-r^2/r_0^2 \right], \quad (9)$$

where coefficients c_{ivs} and c_{ivv} define the strength of isovector-scalar and isovector-vector couplings. For such an interaction the transition operator in (8) is given in the PWA by an analytical expression

$$\hat{\mathcal{O}} \sim \sum_i f_i(q, r_i) \left[c_{ivs} + c_{ivv} \sigma_\mu^{(i)} \right] \tau_-^{(i)} Y_{lm}(\hat{\mathbf{r}}_i),$$

$$f_l(q, r_i) = V_0 r_0^3 \sqrt{2} \pi^2 \exp[-(qr_0/2)^2] j_l(qr_i), \quad (10)$$

where index i numbers the two valence nucleons. Such, relatively simple, choice allowed us to reproduce well the angular distributions of ${}^6\text{Be}$ in Ref. [6].

The exclusive cross section of the direct reaction populating three-body continuum is, in general, an eight-folded differential. In our specific case, when an orientation of the reaction plane does not play a role, we work with a seven-folded differential cross sections and represent it by using the hyperspherical energy variables as

follows

$$\frac{d^7\sigma}{dq dE_T d\Omega_{\mathbf{x}}} = \sum_{SM_S} \sum_{JM, J'M'} \rho_{JM}^{J'M'}(q, E_T) \times A_{JMSM_S}^\dagger(E_T, \Omega_{\mathbf{x}}) A_{J'M'SM_S}(E_T, \Omega_{\mathbf{x}}), \quad (11)$$

where $\rho_{JM}^{J'M'}$ is a density matrix and A_{JMSM_S} are three-body amplitudes depending on the ${}^6\text{Be}$ excitation energy E_T and the five-dimensional hyperspherical “solid angle”

$$\Omega_{\mathbf{x}} = \{\theta_{\kappa}, \hat{\mathbf{k}}_x, \hat{\mathbf{k}}_y\},$$

where $\tan(\theta_{\kappa}) = k_x/k_y$. Here, the slow motion of fragments $\alpha+p+p$ at low excitation energies is described by A_{JMSM_S} amplitudes and the state alignments are contained in the $\rho_{JM}^{J'M'}$.

Note the dependence of the density matrix $\rho_{JM}^{J'M'}$ on the energy E_T and the absolute value of q . In general case there should be a dependence on \mathbf{q} , but the azimuthal angle of \mathbf{q} relative to the beam direction is defined by q and E_T for transfer reactions. Also note that the amplitudes A_{JMSM_S} explicitly depend on E_T and $\Omega_{\mathbf{x}}$, though it can be seen in Eq. (10) that there is also implicit dependence on q . The expression (11) is somewhat different from that stated in Ref. [9] as far as we explicitly provide summation over spin variables $\{S, M_S\}$ of the three-body channel, which are not measurable (at least in foreseen realistic experimental scenarios).

IV. EXPERIMENT

The experiment was performed in the Flerov Laboratory of Nuclear Reaction, Joint Institute for Nuclear Research with the use ACCULINNA setup at U-400M cyclotron [6]. To carry out high efficiency correlation measurements in the charge-exchange reaction ${}^1\text{H}({}^6\text{Li}, {}^6\text{Be})n$, maximal possible statistics of three-particle $\alpha+p+p$ coincidences were desired. This condition required the detection of at least two particles by one of telescopes (see Fig. 2) and the employment of a sophisticated experimental trigger and following data analysis.

The 47 AMeV ${}^6\text{Li}$ beam was produced by the cyclotron U-400M and injected into ACCULINNA facility [10]. The beam energy was reduced to 35 AMeV using a carbon degrader and delivered to the well shielded experimental room, located behind a 2 m thick concrete wall, where the background produced by cyclotron is considerably suppressed.

Experimental target and detectors setup were placed in stainless steel vacuum reaction chamber pumped out to a stationary pressure of $\sim 10^{-6}$ mbar. The beam was focused on experimental target by means of lead diaphragm positioned between two ionization chambers which compare the beam intensity before and after beam passage through the diaphragm. The beam with intensity of about $3 \times 10^7 \text{ s}^{-1}$ was focused to a $\sim 3 \text{ mm}$ (FWHM)

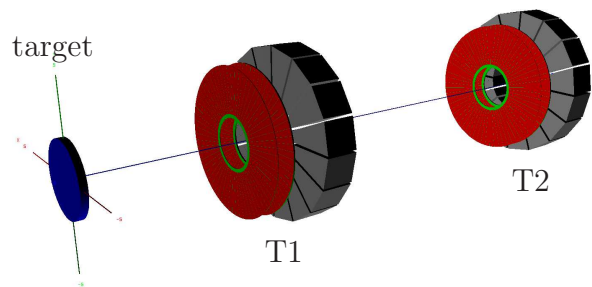


FIG. 2. Schematic view of the detector system employed for registration of the ${}^1\text{H}({}^6\text{Li}, {}^6\text{Be})n$ reaction products. The origin of the left-handed laboratory frame is in the centre of the hydrogen gas target (blue cylinder), each of two identical telescopes (T1 and T2) consists of two position-sensitive Si detectors (red) and the array of CsI(Tl) crystals (grey).

spot in the target plane and an energy spread better than 0.6% was achieved.

The detector array used for registration of the reaction products and a cryogenic hydrogen target are shown schematically in Fig. 2. The 4 mm thick target cell was equipped with 6 μm stainless steel entrance and exit windows. For the sake of the heat shielding this cell was embedded in a protective volume supplied with 2 μm windows of mylar coated with aluminum. The target geometry allowed to detect reaction products emitted in downstream direction with full opening angle of 90° . The target cell was filled with hydrogen gas at a pressure of 3 bar and cooled down to 35 K. The difference between the pressure in target cell and the vacuum chamber caused the inflation of steel windows to lenticular form and resulting at maximal target thickness of 6 mm.

Reaction products were measured by two identical annular telescopes T1 and T2, see Fig. 2. Each telescope consisted of two position-sensitive silicon detectors and an array of 16 trapezoid CsI(Tl) crystals coupled with individual S8650 Si-photodiodes. The first double-sided silicon strip detector (DSSD), 300 μm thick, had 32 sectors on the front side and 32 rings on the back side. The second layer was made of a single-sided silicon strip detector (SSSD) 1 mm thick, segmented into 16 sectors. The inner and outer diameters of the sensitive area of silicon detectors were 32 mm and 82 mm, respectively. The inner diameter of the silicon wafer was 28 mm. The assembly of CsI(Tl) crystals, 19 mm thick, had the inner and outer diameters of 37 mm and 97 mm, respectively. Dead layers of Si detectors were measured using α -source, those of CsI(Tl) detectors were estimated by MC simulations.

Overall thickness of each telescope was sufficient to stop all products of the investigated process with well-defined identification. DSSDs were intended to measure energy loss ΔE of particles (with the threshold of $\sim 300 \text{ keV}$) and the positions of their hits. SSSD and CsI(Tl) detectors served for measurement of the remaining particle energy deposit. Moreover, signals from SSSD were branched to fast time electronic circuit and used

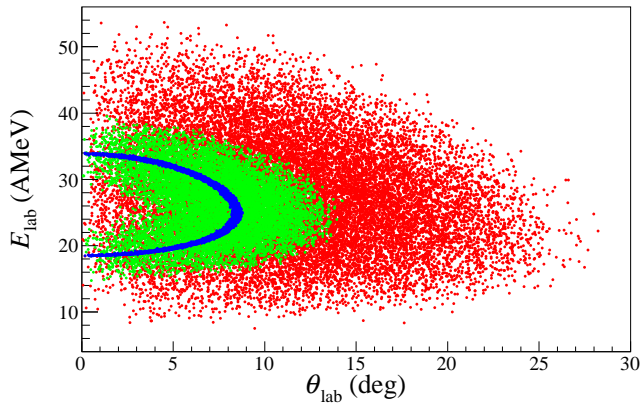


FIG. 3. Kinematic plot of the $^1\text{H}(^6\text{Li},^6\text{Be})n$ reaction and ^6Be decay obtained by MC simulation of the ground and the first excited state population. The beam direction coincides with Z -axis in laboratory frame. θ_{lab} is the polar angle in laboratory frame, E_{lab} is the kinetic energy of the reaction and decay products in the laboratory frame. The ^6Be c.m. is shown by blue dots, α by green dots and protons by red dots.

for formation of the trigger. The telescopes T1 and T2 were placed 91 mm and 300 mm downstream the target, respectively. Under an assumption that the reaction occurred in the center of the target, the T1 and T2 angular ranges in laboratory frame were $9.9^\circ - 24.2^\circ$ and $3.1^\circ - 7.8^\circ$, respectively, see Fig. 3.

V. DATA ANALYSIS

As a result of the experiment the ^6Be energy spectra shown in Figs. 4 (a) and (b) were obtained. The spectrum presented in Fig. 4 (a) consists of two prominent peaks related to the population of the ground 0^+ and the first excited 2^+ states superimposed on the broad continuum. The width of the ground state peak demonstrates overall instrumental resolution. This is a typical picture which has been seen in a number of earlier observations (e.g., see Refs. [11–13]) where the low-energy ^6Be spectrum was populated in charge-exchange reactions. Those results were based on the measurement of the missing mass spectra, and their treatment was often related to the analysis of the excitation spectrum and sometimes its angular behaviour. The detection of three ^6Be products $\alpha+p+p$ provides complete kinematics measurement, and we can consider the population and the decay of the ^6Be system in detail. Below we will focus on the parameters of the model related to the reaction mechanism and how they affect on the measured spectra formation.

The data analysis is performed by comparison of experimental data with Monte-Carlo (MC) simulations based on the three-body decay model taking into account the population of the 0^+ and 2^+ states only, see Section III. Observables relevant to the ^6Be decay will be treated in

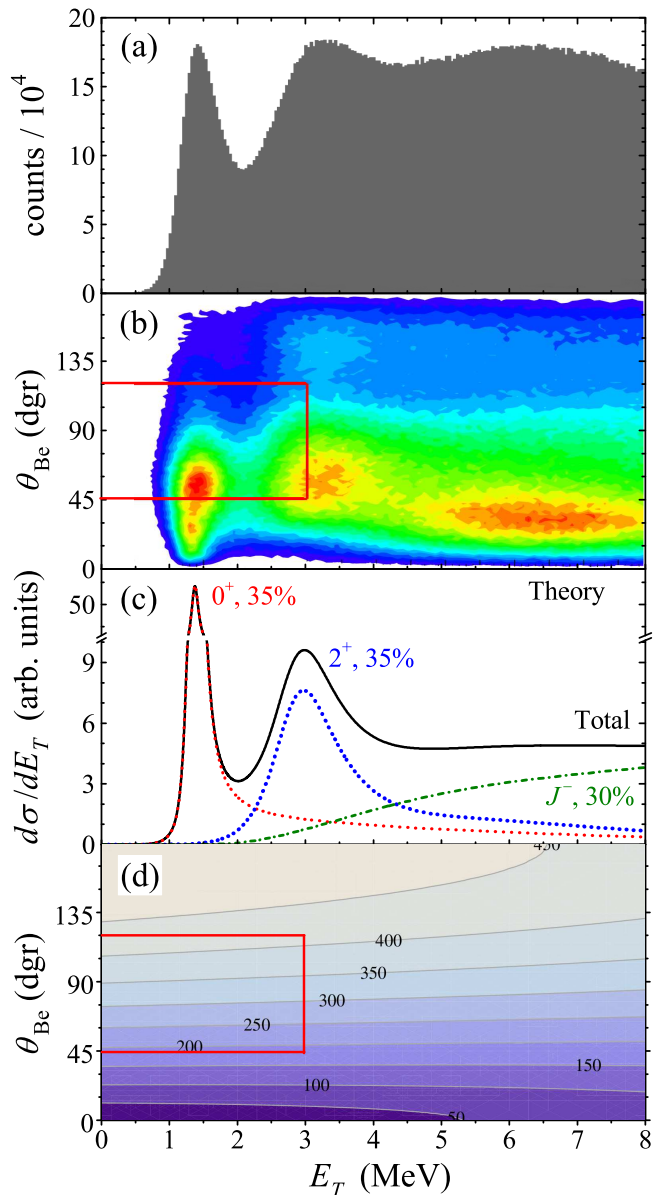


FIG. 4. Experimental data for $^1\text{H}(^6\text{Li},^6\text{Be})n$ reaction. Panel (a) shows the ^6Be integral invariant mass spectrum measured in the whole range of θ_{Be} angle. Panel (b) shows the same data presented on the $\{E_T, \theta_{\text{Be}}\}$ plane. Panel (c) shows theoretical spectra with different J^π and their sum (black solid curve) fitting the data of panels (a) and (b). Panel (d) shows contour plot of the transferred momentum (in MeV/c) on the $\{E_T, \theta_{\text{Be}}\}$ plane. Red rectangle in panels (b) and (d) shows the region of interest for this work.

a specific ^6Be centre-of-mass frame with Z axis directed along the transferred momentum vector.

We have treated our data in the whole angular range of $\theta_{\text{Be}} \in (45, 120)^\circ$ and $E_T < 3.1$ MeV [see rectangle in Fig. 4 (b)]. Both, the ground and first excited states, are well pronounced and are measured with sufficient statistics in this region. At smaller angles setup

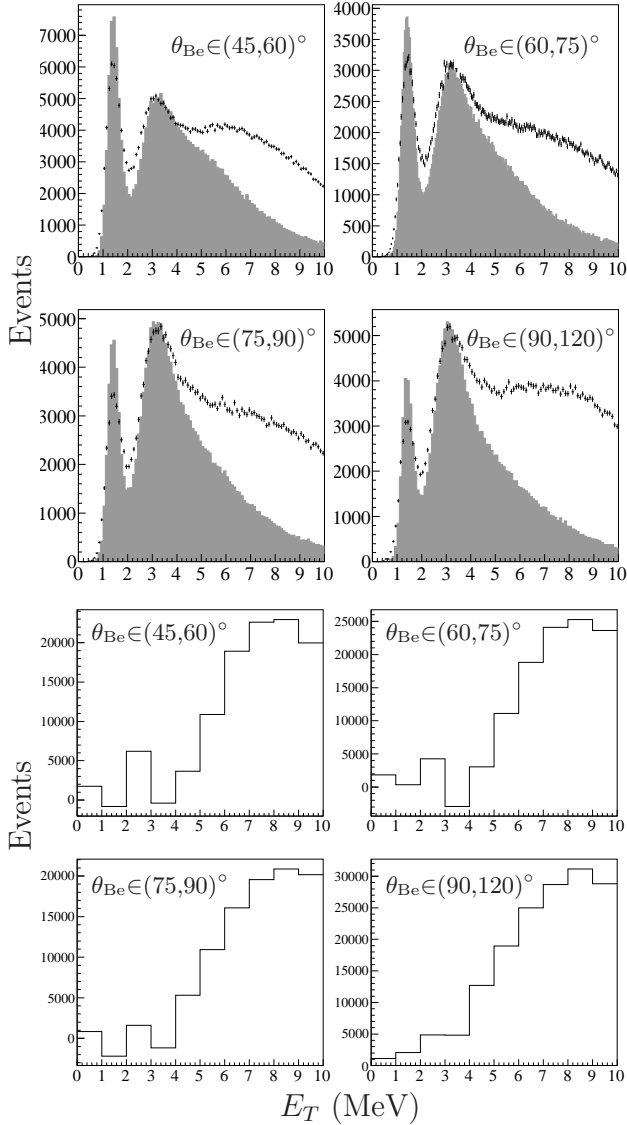


FIG. 5. Comparison experimental data and simulations including 0^+ and 2^+ states in different intervals of θ_{Be} . In four upper panels the experimental and simulated data are depicted by crosses and grey histogram, respectively. In four lower panels the subtraction of experimental and simulated histograms with energy bin of 1 MeV are shown for the same angular ranges. This subtraction shows the expected contributions of J^- states interpreted as isovector soft dipole mode contribution.

efficiency is severely suppressed by the telescope acceptance, while at larger angles population cross section is quite low. The model calculations were passed through a virtual measuring setup taking into account all major details of the experimental setup.

We will attempt to compare theoretical results with experimental data by fitting the three aspects of the density matrix related to investigated states:

- (i) Population ratio of the 0^+ ground state to the 2^+ first excited state;
- (ii) Intensity of the spin-alignment for population of the

2^+ state;

- (iii) Interference phase between of the 0^+ and 2^+ states.

A. Population rates for 0^+ and 2^+

Comparison of the simulated and experimental data in different angular intervals is given in Fig. 5. Experimental and simulated data are depicted by crosses and gray histograms, respectively. We can see that MC simulations overestimates a bit the energy resolution of the experimental setup. For that reason the simulated data were fitted to experimental ones by comparing the numbers of events corresponding to the population of ground state $E_T < 2$ MeV and those forming the left slope of the 2^+ state peak $2.5 < E_T < 3.1$ MeV.

In contrast with treatment of Ref. [6], here we do not include in the MC simulations the contribution of the J^- continuum (Isovector Soft Dipole Mode contribution). Instead, in lower panels of Fig. 5 we show results of the subtraction of simulated 0^+ and 2^+ contributions from the experimental spectrum. We can see that the IVSDM contributions are weakly dependent on the angular range. Another important thing we realize from this illustration is a significant contribution of the IVSDM for the right wing of the 2^+ resonance. This message is confirmed by theoretical calculations of Ref. [6], also shown in Fig. 4 (c). We see that if we would like to study the $0^+/2^+$ mixing only we should stick our analysis mainly to the left wing of the 2^+ resonance with $E_T < 3.1$ MeV.

B. Spin-parity identification and density matrix parametrization

Before we turn to charge exchange-reaction, some explanation how spin-parity identification based on density-matrix formalism was realized in our previous works is needed. The (t,p) reactions were used for population of three-body continuum states in ^5H and ^{10}He in Refs. [4, 5, 14]. Such two-neutron transfer reactions seem to be reliably described by “dineutron” transfer (two nucleons are transferred in a state with $S=0$). Then suppositions about Eq. (2) are fully valid and we get highly aligned density matrix in the transferred momentum frame with practically complete “polar” alignment

$$\rho_{JM}^{J'M'} \sim \delta_{M,\pm 1/2} \delta_{M',\pm 1/2} \quad \text{or} \quad \rho_{JM}^{J'M'} \sim \delta_{M,0} \delta_{M',0}, \quad (12)$$

for half-integer and integer spin of the initial system, respectively. Such strong alignment guarantee very expressed interference patterns for broad overlapping continuum states which were used in the data analysis [4, 5].

In general case the angular distribution of two-body decays is expressed in terms of associated Legendre polynomials $P_L^M(x)$. If a polar-aligned state with angular momentum L decays via emission of particle with $J=0$ the angular distribution of the products may be expressed

as

$$\frac{d\sigma}{d\cos\theta} \sim |P_L^0(\cos\theta)|^2, \quad (13)$$

for the selected alignment system, producing expressed and easy-to-interpret angular distribution.

In the case of the three-body decay, there exist an evident limit effectively reducing three-body motion to two-body motion:

$$\varepsilon \rightarrow 0. \quad (14)$$

When the relative motion of one pair of particles (e.g. two protons) is fully suppressed and the three-body decay is determined as two-body motion of alpha-particle and diproton with zero energy. In this limit we are getting for three-body decays the same very expressed angular distributions, but now in the corresponding β -angle [see Fig. 1(c)].

We introduce the term *quasibinary kinematic* for three-body decay when the condition (14) is replaced by $\varepsilon < x$ assuming a choice made for the upper limit of ε providing satisfactory accuracy for the studied process. For high-statistics measurements the value x can be gradually reduced to reveal expressed and easy-to-interpret correlation patterns.

In our analysis we fix some E_T and θ_{Be} ranges and consider different correlation patterns within them. For internal correlations we consider ε and θ_k distributions and for external correlations the most interesting are angular distributions θ_α of α -particles in the momentum transfer system, $\theta_\alpha = \pi - \beta$.

Formally, the terms of the density matrix $\rho_{JM}^{J'M'}(q, E_T)$ for the pole reaction mechanism in Eq. (11) depend on two parameters: q and E_T . Looking in Fig. 4 (d) it is easy to find that for energy and angular range of our interest momentum transfer depends only on angle, not on energy and thus it is reliable to consider the $\rho_{JM}^{J'M'}$ dependence on E_T and θ_{Be} in a factorized form. So, we presume that:

- (i) The energy profile of the 0^+ and 2^+ states individually is defined by the energy dependence of the three-body amplitudes $A_{JMSM_S}(E_T, \Omega_\pi)$ as provided by three-body theoretical calculations.
- (ii) The “global” population rate for the 0^+ and 2^+ states as fitted to experiment is defined by the parameter $\rho_{00}^{00} / \sum_M \rho_{2M}^{2M}$.
- (iii) The following items are considered separately for each $\{E_T, \theta_{Be}\}$ bin: the alignment for the 2^+ state (ρ_{2M}^{2M} dependence on M) and the “interference angle” φ_{02} between 0^+ and 2^+ states, which define off-diagonal density matrix term parameterised as

$$\rho_{20}^{00} = \rho_{00}^{20} = \sqrt{\rho_{00}^{00} \rho_{20}^{20}} \cos(\varphi_{02}). \quad (15)$$

The expected alignment pattern for the ${}^6\text{Be}$ 2^+ state populated in the charge-exchange reaction induced by the potential Eq. (9) is illustrated in Fig. 6 (a). Actually,

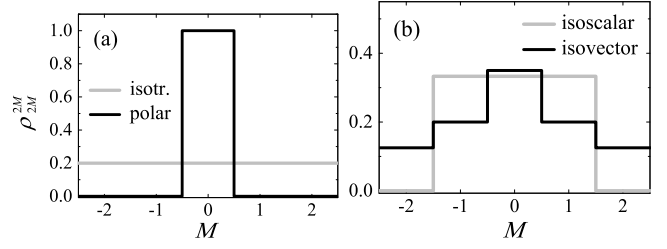


FIG. 6. The density matrix (11) spin structure for the 2^+ state. (a) Model approximations of isotropic and polar alignments actually used for MC simulations. (b) Isovector-scalar (constant c_{ivs}) and isovector-vector (constant c_{ivv}) couplings for potential (9).

more expressed alignment parameterizations were used for the MC simulations. Expressions

$$\rho_{2M} \sim \delta_{M0}, \quad (16)$$

$$\rho_{2M} \sim 1/5, \quad (17)$$

correspond to population of fully polar-aligned (16) and nonaligned (isotropic) (17) 2^+ state, respectively. If we consider the angular distribution of α -particle fragment in the momentum transfer frame, then the isotropic density matrix should provide isotropic angular distribution for the isolated 2^+ state. Note that in the case of significant interference with other states an anisotropic distribution can be obtained even for isotropically populated state. With increase of the alignment more and more distinctive form of angular distribution should be obtained for the 2^+ state, tending to $|P_2^0(\cos\theta_\alpha)|^2$ in the limit of polar alignment and the under the condition (14).

Three extreme cases of interference between $0^+/2^+$, described by angle φ_{02} , are considered. We simulated the constructive interference ($\varphi_{02}=0^\circ$), destructive interference ($\varphi_{02}=180^\circ$) and situation when amplitudes of 0^+ and 2^+ states are summed incoherently ($\varphi_{02}=90^\circ$) for both cases determined by equations (16) and (17).

So, within this paper, six special cases are systematically illustrated, those given by two extreme cases of 2^+ alignment and three distinct cases of $0^+/2^+$ interference, see e.g. Fig. 7.

C. Ground state correlations

We start our analysis from the part of the ${}^6\text{Be}$ excitation spectrum where the 0^+ ground state is only present. To eliminate the possible effects caused by the interference with the 2^+ state we restricted analysis here to excitation energy $E_T \leq 1.4 \text{ MeV}$, where contribution of the left “wing” of the first excited state can be reliably neglected. So, we have no free model parameters related to the reaction mechanism (0^+ state by itself is “isotropic” by definition) there and internal correlations of ${}^6\text{Be}$ decay products should be the same for the whole range of angle θ_{Be} .

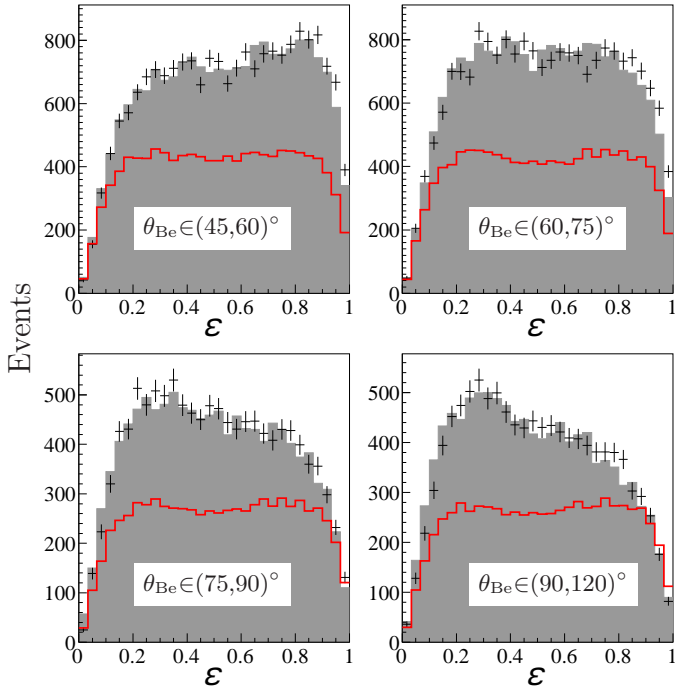


FIG. 7. Energy distributions ε_T for ${}^6\text{Be}$ decay with $E_T < 1.4$ MeV for different θ_{Be} bins. Experimental and simulated data are depicted by crosses and grey histograms, respectively. Theoretical input is illustrated by red lines.

We can see in Fig. 7 that observed ε_T distributions are qualitatively different for different θ_{Be} bins. In spite of this fact the simulated energy distributions (gray histograms) are in a nice agreement with experimental data (theoretical distributions depicted by red histograms are the same for all panels in Fig. 7).

The effect of the response of the experimental setup is much smaller for ε_Y distribution in the “Y”-system and $\cos\theta_k^{(T)}$ in the “T”-system. It also only very weakly depending on the kinematical range of θ_{Be} . In Fig. 8 we show typical picture of these distributions. Corrections induced by detection efficiency are noticeable, but not large.

Analysis of internal correlations for the ground state given here may be seen as a benchmark in two ways. On the one hand, it provides a confirmation of the theoretically predicted correlations, which were already tested against highly detailed experimental data of works [15, 16]. Thus, the full consistency of our experiment with previous high-precision experiments [15, 16] is demonstrated. On the other hand, the nice agreement in Figs. 7 and 8 means that the MC simulation is working reliably in the whole considered θ_{Be} range and well represents response of the experimental setup. This is an important prerequisite for the next more complicated steps of our analysis.

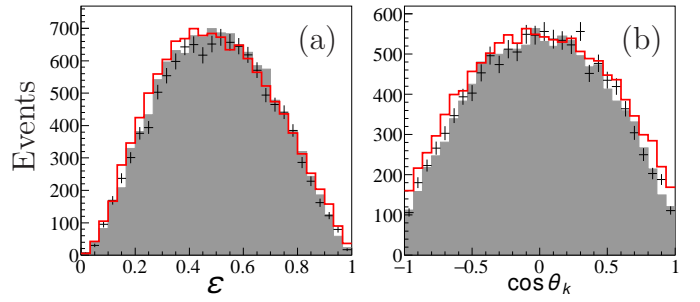


FIG. 8. Panel (a) shows energy distributions ε_Y in the Jacobi “Y”-system. Panel (b) shows angular distribution $\cos\theta_k^{(T)}$ in the Jacobi “T”-system. Kinematical range $E_T < 1.4$ MeV and $75^\circ < \theta_{\text{Be}} < 90^\circ$.

D. Correlations at the right slope of the 0^+ state

Effects of $0^+/2^+$ interference become important already on the right slope of the ground 0^+ state. Let us have a look at the energy range $1.4 < E_T < 1.9$ MeV. If we look in theoretical predictions shown in Fig. 4 (c), we can find that the relative probability of the 2^+ state population expected in this energy range is just around 1% of the 0^+ one. Nevertheless, it is sufficient to produce a significant modification in the correlations. This is the important motivation for use of correlations as a tool for studies: they are sensitive to amplitudes, not to probabilities. Therefore, the effects of even small-weight configurations can be drastically amplified.

First, we consider the evolution of energy ε_T distributions with angle θ_{Be} . It is illustrated in Fig. 9 for the “trivial” case of isotropic and not interfering 2^+ state. The calculated distributions are not much different from the ones shown in Fig. 7 and evidently do not depend on the angle θ_{Be} . However, observable ε_T distributions are strongly sensitive to the angle θ_{Be} and we can see that MC simulations are reliably taking the experimental efficiency into account in this range as well.

Much more fine effect of the alignment/interference on the energy distribution ε_T is illustrated in Fig. 10. We can see in this plot that there is weak dependence of the *observed* shape of the distribution on the alignment/interference settings. Please note that from theoretical point of view there is no dependence of the ε_T distributions on the reaction mechanism. However, such a sensitivity of *observable* distributions arise in the experimental conditions, when isotropic efficiency for registration of decay fragments is not available. This effect has been already pointed in Ref. [17] (see Fig. 6 of this work) for the ${}^6\text{Be}$ 2^+ data from experiment [16].

The dependence of Fig. 10 is quite curious, but too weak for practical application and deriving definite conclusions. To distinguish clearly the effects of alignment/interference it is better to consider external correlations in the momentum transfer frame. Angular distributions for α -particle emission in the momentum transfer

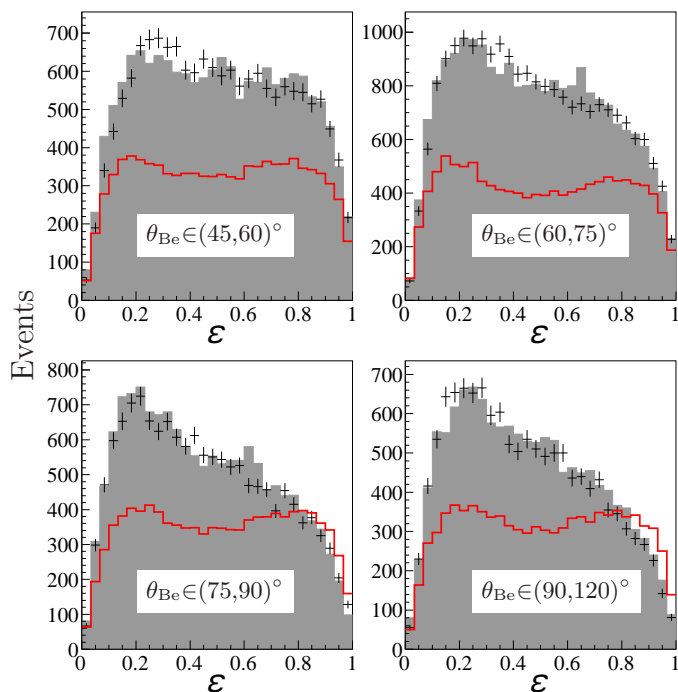


FIG. 9. Energy distribution ε_T for ${}^6\text{Be}$ decay with $1.4 < E_T < 1.9$ MeV (right slope of 0^+) for different θ_{Be} bins. The simulation model settings are isotropic 2^+ state (NA) and no $0^+/2^+$ interference ($\varphi_{02} = 90^\circ$).

frame are illustrated in Fig. 11. We analysed the ${}^6\text{Be}$ decay in quasibinary approximation under the condition

$$\varepsilon_T < 0.2, \quad (18)$$

which ensured high enough statistics for the considered $\{E_T, \theta_{\text{Be}}\}$ windows. It can be seen in Fig. 11 that already theoretical angular distributions are very sensitive to alignment/interference conditions. This sensitivity is further enhanced by imperfect experimental efficiency. It is clear that these distributions can be used to fix alignment/interference parameters with reasonable confidence. The analysis analogous to that of Fig. 11 was performed in the whole θ_{Be} range and the results are summarized in Table I.

Note, that such a strong sensitivity of the observed angular distributions is obtained just for $\sim 1\%$ of the 2^+ state relative weight in the considered E_T energy window.

E. Correlations at the left slope of the 2^+ state

We may expect that effects of alignment/interference will be more pronounced in the region with higher probability of population of the 2^+ state. As illustration we provide here some details for the range $2.5 < E_T < 3.1$ MeV. This corresponds to the left (rising) slope of the first excited 2^+ state of ${}^6\text{Be}$. It can be expected from Fig. 4 (c) $\sim 20\%$ of 0^+ contribution in this

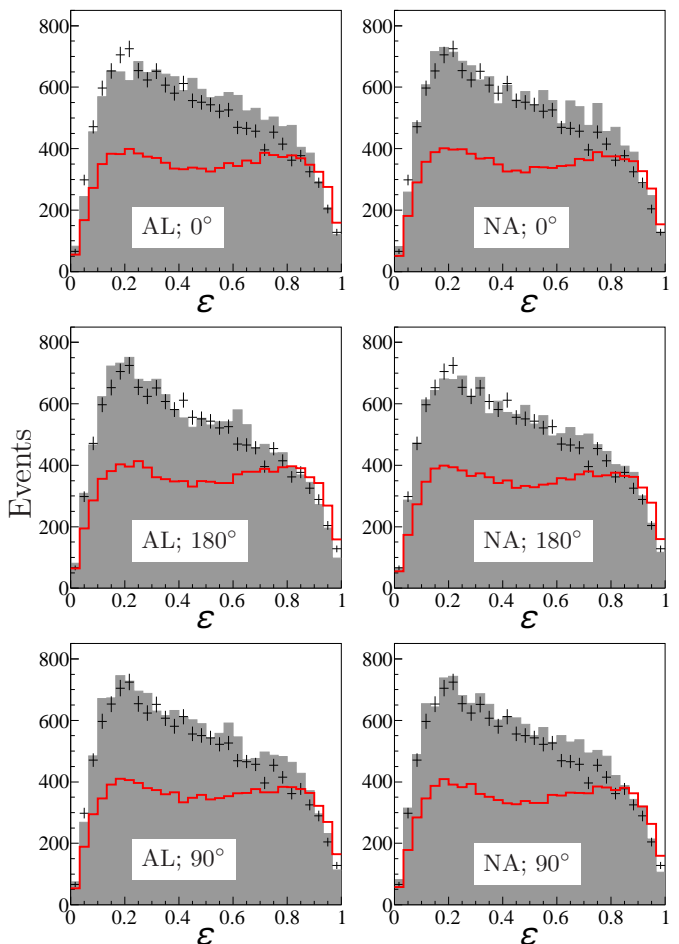


FIG. 10. Energy distributions ε_T for ${}^6\text{Be}$ decay with $1.4 < E_T < 1.9$ MeV (right slope of 0^+) for $75^\circ < \theta_{\text{Be}} < 90^\circ$ and different alignment/interference settings. The left column, compares data with theoretical model describing fully polar-aligned (AL) 2^+ state. The right column, corresponds to the isotropic (nonaligned, NA) 2^+ state. Upper, middle, and bottom rows correspond to interference phase φ_{02} equal to 0° , 180° , and 90° , respectively.

range making strong interference highly probable. Certain “contamination” of the correlations in this range by J^- contributions can be expected, but analysis shows that in reality it appears to be not of importance. Thus, the analysis scheme here is quite stereotypical with that of the previous Section.

Our first test is energy distribution ε_T , which gives minimal validation of the MC procedure quality, see Fig. 12. This energy distribution for the 2^+ state is qualitatively different from that for the 0^+ state. The major effects of experimental response are effectively removed by MC simulations shown in Fig. 12. More fine effects of the alignment/interference on the observable distributions are illustrated for the selected θ_{Be} range in Fig. 13.

All other distributions related to internal correlations, θ_k in both “Y” and “T” systems and ε_Y show the same nice agreement between experiment and theory. As a

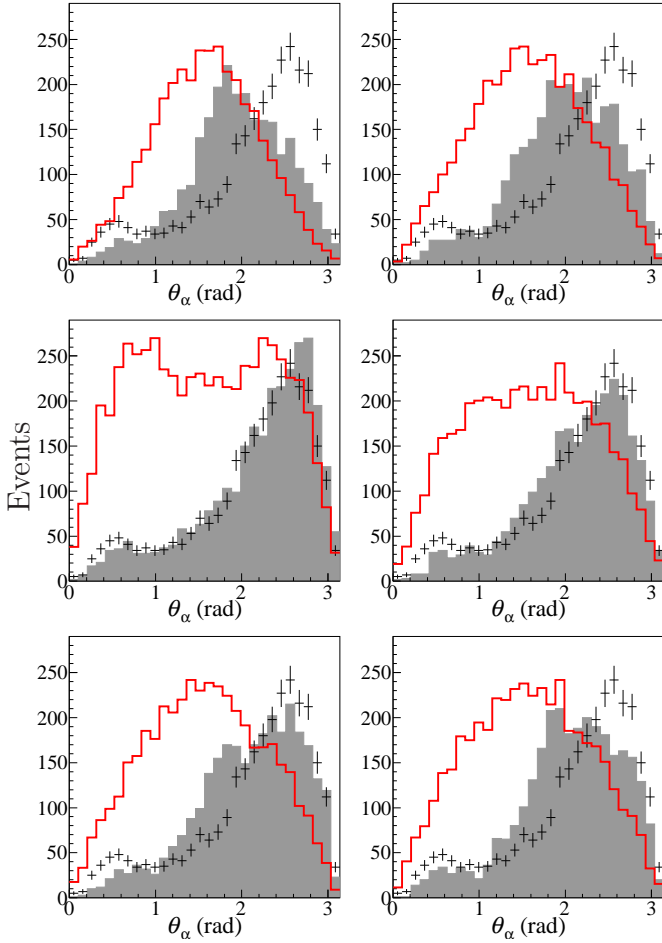


FIG. 11. Angular distributions for the α -particle emission in the momentum transfer frame in the range $1.4 < E_T < 1.9$ MeV and $75^\circ < \theta_{Be} < 90^\circ$. Alignment/interference settings are the same as in Fig. 10.

result of these studies we can declare two observations:

- (i) The internal correlations do not seem to demonstrate noticeable dependence on the population conditions. This is a quite expected result for the narrow 0^+ state ($\Gamma \approx 90$ keV), however, for much broader 2^+ state ($\Gamma \sim 1$ MeV) this is not evident in advance. Thus, the internal motion of the three-body system seems to be really disentangled from the motion of the three-body system as a whole as it is presumed in the density matrix formalism.
- (ii) The same theoretical input for the 2^+ state correlations was used for MC simulations in Ref. [16]. As far as the agreement between theory and experiment was also very good in this work, it means that there is a complete agreement between this experiment and the experiment [16]. The ${}^6\text{Be}$ states were populated in a high-energy ($E_{\text{beam}} \sim 70$ A MeV) knockout from ${}^7\text{Be}$ beam in experiment [16]. This is very different reaction mechanism, so the internal correlations in the decay of relatively broad 2^+ state seem to be not sensitive also to this aspect of

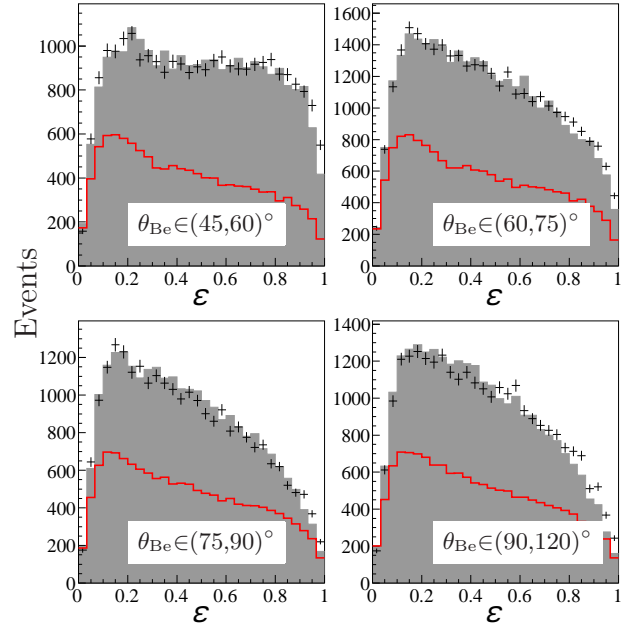


FIG. 12. Energy distribution ϵ_T for the ${}^6\text{Be}$ decay with $2.5 < E_T < 3.1$ MeV (left slope of 2^+) for different θ_{Be} bins. The simulation model settings are isotropic 2^+ state (NA) and no $0^+/2^+$ interference ($\varphi_{02} = 90^\circ$).

the reaction mechanism.

The analysis of external correlations is illustrated by Figs. 14 and 15 for two selected θ_{Be} ranges. Again the sensitivity of the θ_α angular distributions to the alignment/interference conditions is very high. However, we can find the density matrix parameters for which near perfect description of the distribution is provided. The results of our fits are summarized in the Table I. Part of the spectrum characterized by pure ground state ($E_T < 1$ MeV) does not depend on the density matrix parameters and it is not shown in the Table.

F. Correlations at the right slope of the 2^+ state

Let us consider now the energy range $3.1 < E_T < 3.7$ MeV. It has been discussed above in the Section V A that important contribution IVSDM is expected here. Inclusive contribution of J^- states here can be theoretically evaluated as $\sim 25\%$ from Fig. 4 (c). How this fact is reflected in the correlations?

The typical picture of comparison of theoretical data with experimental ones for energy above the peak corresponding to the 2^+ state is shown in Fig. 16. It is obvious that experimental data cannot be fitted using 0^+ and 2^+ contributions only because of the simulated events excess for all model interference/alignment settings at $\theta_\alpha \sim \pi/2$. Moreover, it is clear that forward/backward asymmetry in the data is much higher than in the simulations. Such a forward/backward asymmetry is not possible for isolated states or for interference of states with the same parity.

TABLE I. The best fit to experimental data of density matrix parameters for different $\{E_T, \theta_{Be}\}$ ranges. The fits were found using the figures with θ_α distribution for all six configurations of the theoretical model.

E_T (MeV)	$\theta_{Be} \in (45, 60)^\circ$	$\theta_{Be} \in (60, 75)^\circ$	$\theta_{Be} \in (75, 90)^\circ$	$\theta_{Be} \in (90, 120)^\circ$
1.4–1.9	AL; $\varphi_{02}=135^\circ$	AL + 50% NA; $\varphi_{02}=180^\circ$	AL; $\varphi_{02}=180^\circ$	AL + 20% NA; $\varphi_{02}=180^\circ$
1.9–2.5	AL + 50% NA; $\varphi_{02}=135^\circ$	NA + 10% AL; $\varphi_{02}=180^\circ$	NA; $\varphi_{02}=180^\circ$	AL + 10% NA; $\varphi_{02}=90^\circ$
2.5–3.1	NA + 10% AL; $\varphi_{02}=180^\circ$	AL + 10% NA; $\varphi_{02}=180^\circ$	NA + 30% AL; $\varphi_{02}=90^\circ$	NA; $\varphi_{02}=135^\circ$

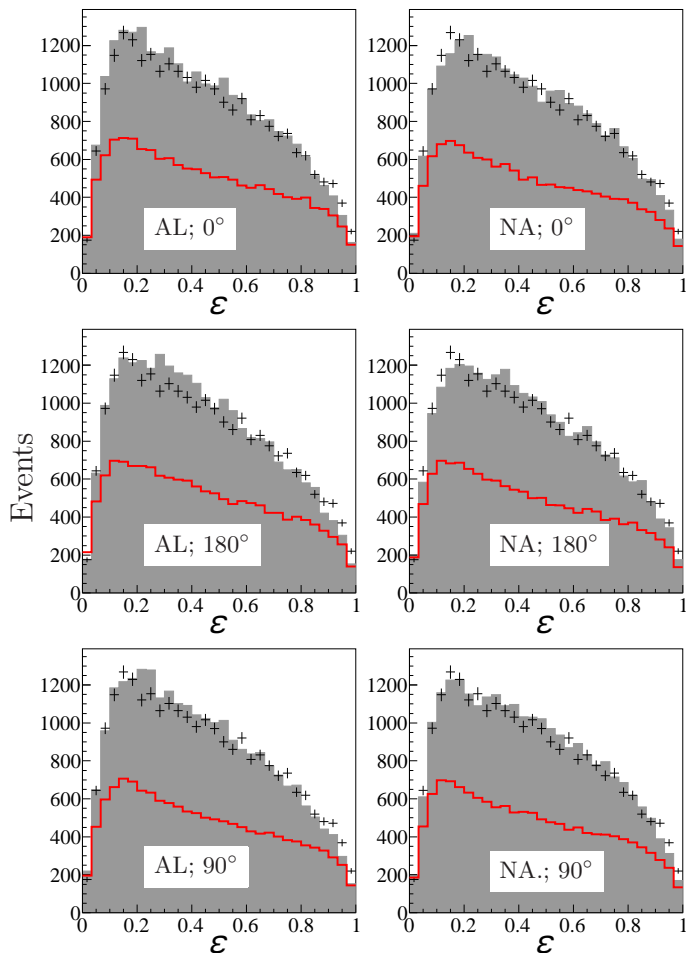


FIG. 13. Energy distribution ε_T for ${}^6\text{Be}$ decay with $2.5 < E_T < 3.1$ MeV (left slope of 2^+) for $75^\circ < \theta_{Be} < 90^\circ$ and different alignment/interference settings, see also caption of the Fig. 10 for details.

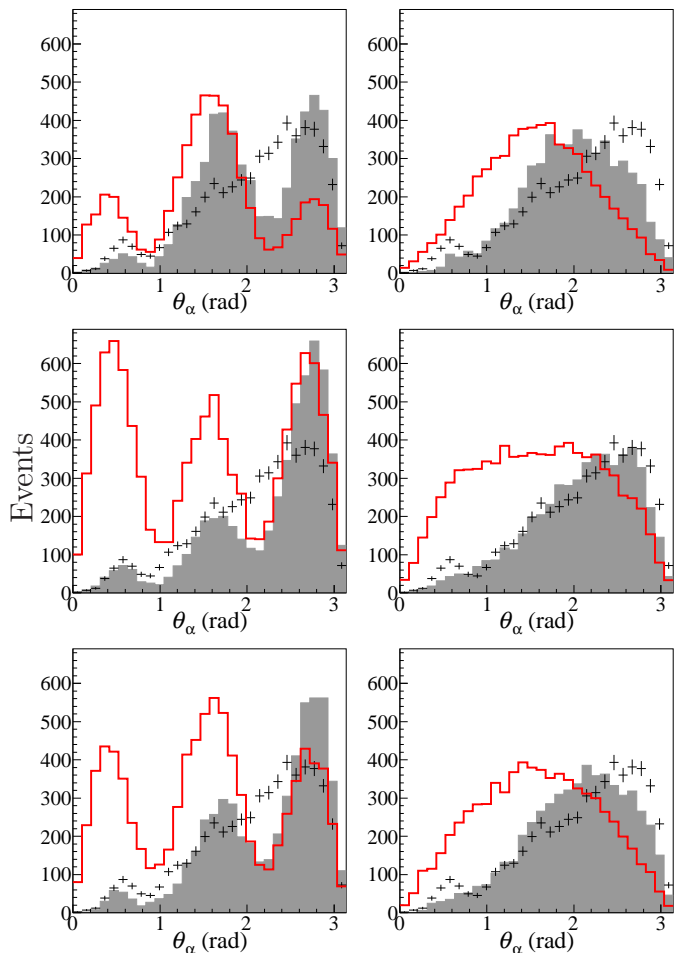


FIG. 14. Angular distributions for the α -particle emission in the momentum transfer frame in the range $2.5 < E_T < 3.1$ MeV and $75^\circ < \theta_{Be} < 90^\circ$. Alignment/interference settings are the same as in Fig. 10.

VI. DISCUSSION

This means that asymmetry obtained in the simulations can be related only to the response of the experimental setup. Simulations show that this effect is not sufficient to explain the observed forward/backward asymmetry. It means that additional interference of 0^+ and 2^+ with some J^- states is needed for explanation of the data. This can be seen as additional independent proof of the IVSDM contribution at $E_T > 3$ MeV.

Studies of the three-body correlations for decays [18–20] or particle emission from states populated in reactions [3–5, 21, 22] are quite active in the recent years. In such studies the experimental question arises, which should be resolved to make theoretical interpretation possible: how much the *observed* correlation patterns are different from the *actual*? In this work we provide extensive illustration of this issue: even for the ${}^6\text{Be}$ ground

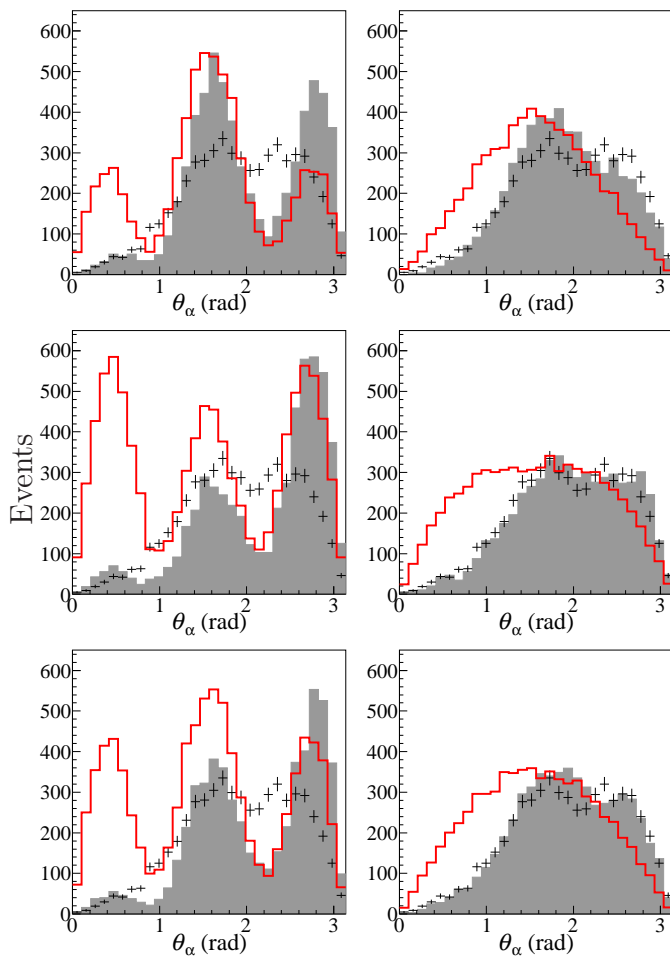


FIG. 15. Angular distributions for the α -particle emission in the momentum transfer frame in the range $2.5 < E_T < 3.1$ MeV and $90^\circ < \theta_{\text{Be}} < 120^\circ$. Alignment/interference settings are the same as in Fig. 10.

state case, the observed three-body correlation patterns demonstrate strong variation depending on the specific region of the kinematical space. The influence of the experimental efficiency is especially harmful for studies of the external correlations. In this work we disentangle the effects related to response of the experimental setup from the effects of alignment/interference for energy range where 0^+ and 2^+ states of ${}^6\text{Be}$ effectively overlap.

A general quantum-mechanical formal issue and important practical task of data interpretation is the extraction of the *most complete* quantum-mechanical information from the accessible observables. Important but very rare case when extraction of the *complete* quantum-mechanical information from data is possible is elastic scattering: from angular distributions one can, in principle, extract set of phase shifts which contains all possible information about this process. For other classes of experimental data extraction of complete quantum-mechanical information from observables suffers from dif-

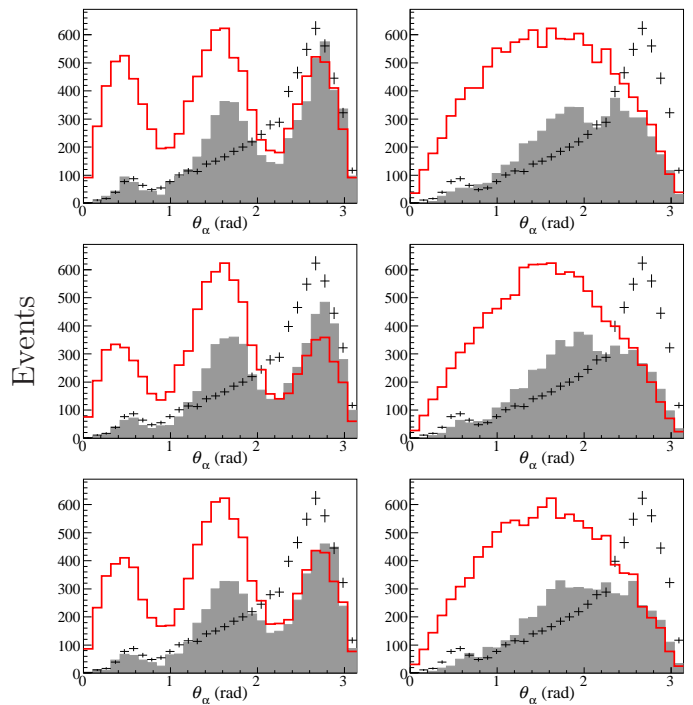


FIG. 16. Angular distribution of α -particles in the momentum transfer frame for the range $3.1 < E_T < 3.7$ MeV and $75^\circ < \theta_{\text{Be}} < 90^\circ$. Alignment and interference conditions are the same as in Fig. 10.

ferent types of continuous and discrete ambiguities. For certain classes of reactions the *most complete* quantum-mechanical information which can be extracted is contained in the density matrix. Because of internal symmetries the density matrix could provide very compact form of data representation depending just on very few parameters. In the case of the pole approximation considered for the ${}^1\text{H}({}^6\text{Li}, {}^6\text{Be})n$ reaction there are just four parameters for specific kinematical point: the $0^+/2^+$ ratio, the $0^+/2^+$ relative phase, and two parameters describing 2^+ state alignment. The density matrix approximation may be questioned for such complicated process as charge-exchange reaction. Despite this issue we demonstrate in this work principal ability to describe very complex and detailed multi-dimensional correlation patterns by applying this compact formalism.

In the mentioned recent three-body correlation studies, the detailed correlation data allowed to resolve the following intriguing questions.

- (i) It was possible to check consistency of the long-range aspect of the three-body problem in continuum [19, 21].
- (ii) We were able to figure out fine details of the decay dynamics for democratic decays by examples of ${}^6\text{Be}$ and ${}^{16}\text{Ne}$ ground and first excited states [15, 21, 22].
- (iii) Possibility to uncover weakly populated states due to interference with “background” states was demonstrated in [3, 4].

In this work we add one more point to this list of sci-

entific tasks which can be resolved by correlation studies. The basic point here is that correlation data are *very detailed* to make possible investigation in different regions of the kinematical space. Such a detailed information is not easily accessible in exotic dripline systems where secondary beams typically have low or modest intensities. Our work provide additional motivation for this type of reaction studies.

VII. CONCLUSIONS

The correlation data for three-body $\alpha+p+p$ decay of the ${}^6\text{Be}$ continuum with overlapping states populated in the ${}^1\text{H}({}^6\text{Li}, {}^6\text{Be})n$ charge-exchange reaction were analyzed. The energy region $E_T < 3\text{ MeV}$, where low-lying 0^+ and 2^+ states are populated, has been considered. Experimental data of high statistics ($\sim 5 \times 10^6$ reconstructed events) allowed us to investigate correlations with reasonable resolution both in the ${}^6\text{Be}$ excitation energy and in the reaction center-of-mass angle. Data analysis was carried out by using the comparison of experimental data with MC simulations taking into account the population of 0^+ and 2^+ states in the ${}^6\text{Be}$ continuum and neglecting the population of J^- continuum. Our treatment showed that internal structure of three-body system with broad overlapping states may be revealed in correlations. While internal correlations are weakly sensitive to the investigated parameters (interference between the 0^+ and 2^+

states and alignment of 2^+ state), we observed strong sensitivity to those parameters in external correlations.

The principal opportunity to extract the density-matrix parameters, characterizing the reaction mechanism of population of the ${}^6\text{Be}$ states, was demonstrated. The suggested method of analysis allows for identification of such fine effects like the ratio of the populated states, interference between them and alignment of the states with $J > 1/2$ for other nuclei, and it may be regarded as a general tool for similar tasks.

Nice examples of the employment of the three-body correlations for spin-parity identification are high-statistics experimental file ${}^5\text{H}$ [3, 4], low-statistics set ${}^{10}\text{He}$ [5] and high-precision treatment of the three-body Coulomb continuum effects in ${}^{16}\text{Ne}$ [21]. The results obtained in this work provide exemplary demonstration how the high-statistics few-body correlation data can be used for determination of the fine effects of the reaction mechanism. This work underline the importance of the high-statistics studies of the few-body correlations as important point of experimental agenda of RIB facilities.

VIII. ACKNOWLEDGEMENTS

This work was partly supported by Russian Science Foundation (grant No. 17-12-01367) and MEYS Projects (Czech Republic) LTT17003 and LM2015049.

-
- [1] K. P. Artemov *et al.*, Sov. J. Nucl. Phys. **14**, 615 (1972), [Yad. Fiz. **14** (1972) 1105]. Parity violation in ${}^6\text{Li}$ 0^+ . Experiment.
 - [2] M. S. Golovkov, L. V. Grigorenko, G. M. Ter-Akopian, A. S. Fomichev, Y. T. Oganessian, V. A. Gorshkov, S. A. Krupko, A. M. Rodin, S. I. Sidorchuk, R. S. Slepnev, S. V. Stepantsov, R. Wolski, D. Y. Pang, V. Chudoba, A. A. Korshennikov, E. A. Kuzmin, E. Y. Nikolskii, B. G. Novatskii, D. N. Stepanov, P. Roussel-Chomaz, W. Mittig, A. Ninane, F. Hanappe, L. Stuttgé, A. A. Yukhimchuk, V. V. Perevozchikov, Y. I. Vinogradov, S. K. Grishechkin, and S. V. Zlatoustovskiy, Phys. Lett. B **672**, 22 (2009).
 - [3] M. S. Golovkov, L. V. Grigorenko, A. S. Fomichev, S. A. Krupko, Y. T. Oganessian, A. M. Rodin, S. I. Sidorchuk, R. S. Slepnev, S. V. Stepantsov, G. M. Ter-Akopian, R. Wolski, M. G. Itkis, A. A. Bogatchev, N. A. Kondratiev, E. M. Kozulin, A. A. Korshennikov, E. Y. Nikolskii, P. Roussel-Chomaz, W. Mittig, R. Palit, V. Bouchat, V. Kinnard, T. Materna, F. Hanappe, O. Dorvaux, L. Stuttgé, A. A. Yukhimchuk, V. V. Perevozchikov, Y. I. Vinogradov, S. K. Grishechkin, S. V. Zlatoustovskiy, V. Lapoux, R. Raabe, and L. Nalpas, Phys. Rev. Lett. **93**, 262501 (2004).
 - [4] M. S. Golovkov, L. V. Grigorenko, A. S. Fomichev, S. A. Krupko, Y. T. Oganessian, A. M. Rodin, S. I. Sidorchuk, R. S. Slepnev, S. V. Stepantsov, G. M. Ter-Akopian, R. Wolski, M. G. Itkis, A. A. Bogatchev, N. A. Kondratiev, E. M. Kozulin, A. A. Korshennikov, E. Y. Nikolskii, P. Roussel-Chomaz, W. Mittig, R. Palit, V. Bouchat, V. Kinnard, T. Materna, F. Hanappe, O. Dorvaux, L. Stuttgé, A. A. Yukhimchuk, V. V. Perevozchikov, Y. I. Vinogradov, S. K. Grishechkin, S. V. Zlatoustovskiy, V. Lapoux, R. Raabe, and L. Nalpas, Phys. Rev. C **72**, 064612 (2005).
 - [5] S. I. Sidorchuk, A. A. Bezbakh, V. Chudoba, I. A. Egorova, A. S. Fomichev, M. S. Golovkov, A. V. Gorshkov, V. A. Gorshkov, L. V. Grigorenko, P. Jalůvková, G. Kaminski, S. A. Krupko, E. A. Kuzmin, E. Y. Nikolskii, Y. T. Oganessian, Y. L. Parfenova, P. G. Sharov, R. S. Slepnev, S. V. Stepantsov, G. M. Ter-Akopian, R. Wolski, A. A. Yukhimchuk, S. V. Filchagin, A. A. Kirdyashkin, I. P. Maksimkin, and O. P. Vikhlyantsev, Phys. Rev. Lett. **108**, 202502 (2012).
 - [6] A. Fomichev, V. Chudoba, I. Egorova, S. Ershov, M. Golovkov, A. Gorshkov, V. Gorshkov, L. Grigorenko, G. Kaminski, S. Krupko, I. Mukha, Y. Parfenova, S. Sidorchuk, R. Slepnev, L. Standlyo, S. Stepantsov, G. Ter-Akopian, R. Wolski, and M. Zhukov, Physics Letters B **708**, 6 (2012).
 - [7] S. Treiman and C. Yang, Phys. Rev. Lett. **8**, 140 (1962).
 - [8] I. Shapiro, V. Kolybasov, and G. Augst, Nucl. Phys. **61**, 353 (1965).
 - [9] L. V. Grigorenko, I. A. Egorova, R. J. Charity, and M. V. Zhukov, Phys. Rev. C **86**, 061602 (2012).

- [10] A. M. Rodin, S. I. Sidorchuk, S. V. Stepantsov, G. M. Ter-Akopian, A. S. Fomichev, R. Wolski, V. B. Galinskiy, G. N. Ivanov, I. B. Ivanova, V. A. Gorshkov, A. Y. Lavrentev, and Y. T. Oganessian, *Nuclear Instruments and Methods in Physics Research A* **391**, 229 (1997).
- [11] D. Tilley, C. Cheves, J. Godwin, G. Hale, H. Hofmann, J. Kelley, C. Sheu, and H. Weller, *Nucl. Phys.* **A708**, 3163 (2002).
- [12] X. Yang, L. Wang, J. Rapaport, C. Goodman, C. Foster, Y. Wang, E. Sugarbaker, D. Marchlinski, S. de Lucia, B. Luther, L. Rybarczyk, T. Taddeucci, and B. Park, *Phys. Rev. C* **52**, 2535 (1995).
- [13] V. Guimaraes, R. Kuramoto, R. Lichtenhaler, G. Amadio, E. Benjamin, P. de Faria, A. Lepine-Szily, G. Lima, J. Kolata, G. Rogachev, F. Becchetti, T. O'Donnell, Y. Chen, J. Hinnefeld, and J. Lapton, *Nucl. Phys. A* **722**, C341C346 (2003).
- [14] M. S. Golovkov, L. V. Grigorenko, A. S. Fomichev, Y. T. Oganessian, Y. I. Orlov, A. M. Rodin, S. I. Sidorchuk, R. S. Slepnev, S. V. Stepantsov, G. M. Ter-Akopian, and R. Wolski, *Phys. Lett. B* **588**, 163 (2004).
- [15] L. V. Grigorenko, T. D. Wiser, K. Mercurio, R. J. Charity, R. Shane, L. G. Sobotka, J. M. Elson, A. H. Wuosmaa, A. Banu, M. McCleskey, L. Trache, R. E. Tribble, and M. V. Zhukov, *Phys. Rev. C* **80**, 034602 (2009).
- [16] I. A. Egorova, R. J. Charity, L. V. Grigorenko, Z. Chajewski, D. Coupland, J. M. Elson, T. K. Ghosh, M. E. Howard, H. Iwasaki, M. Kilburn, J. Lee, W. G. Lynch, J. Manfredi, S. T. Marley, A. Sanetullaev, R. Shane, D. V. Shetty, L. G. Sobotka, M. B. Tsang, J. Winkelbauer, A. H. Wuosmaa, M. Youngs, and M. V. Zhukov, *Phys. Rev. Lett.* **109**, 202502 (2012).
- [17] L. V. Grigorenko, I. G. Mukha, and M. V. Zhukov, *Phys. Rev. Lett.* **111**, 042501 (2013).
- [18] K. Miernik, W. Dominik, Z. Janas, M. Pfützner, L. Grigorenko, C. R. Bingham, H. Czyrkowski, M. Cwiok, I. G. Darby, W. Dominik, J. M. Elson, T. Ginter, R. Grzywacz, Z. Janas, M. Karny, A. Korgul, S. N. Liddick, K. Rykaczewski, and A. Stolz, *Phys. Rev. Lett.* **99**, 192501 (2007).
- [19] L. V. Grigorenko, T. D. Wiser, K. Miernik, R. J. Charity, M. Pfützner, A. Banu, C. R. Bingham, M. Cwiok, I. G. Darby, W. Dominik, J. M. Elson, T. Ginter, R. Grzywacz, Z. Janas, M. Karny, A. Korgul, S. N. Liddick, K. Mercurio, M. Rajabali, K. Rykaczewski, R. Shane, L. G. Sobotka, A. Stolz, L. Trache, R. E. Tribble, A. H. Wuosmaa, and M. V. Zhukov, *Phys. Lett. B* **677**, 30 (2009).
- [20] P. Ascher, L. Audirac, N. Adimi, B. Blank, C. Borcea, B. A. Brown, I. Companis, F. Delalee, C. E. Demonchy, F. de Oliveira Santos, J. Giovinazzo, S. Grévy, L. V. Grigorenko, T. Kurtukian-Nieto, S. Leblanc, J.-L. Pedroza, L. Perrot, J. Pibernat, L. Serani, P. C. Srivastava, and J.-C. Thomas, *Phys. Rev. Lett.* **107**, 102502 (2011).
- [21] K. W. Brown, R. J. Charity, L. G. Sobotka, Z. Chajewski, L. V. Grigorenko, I. A. Egorova, Y. L. Parfenova, M. V. Zhukov, S. Bedoor, W. W. Buhro, J. M. Elson, W. G. Lynch, J. Manfredi, D. G. McNeel, W. Reviol, R. Shane, R. H. Showalter, M. B. Tsang, J. R. Winkelbauer, and A. H. Wuosmaa, *Phys. Rev. Lett.* **113**, 232501 (2014).
- [22] K. W. Brown, R. J. Charity, L. G. Sobotka, L. V. Grigorenko, T. A. Golubkova, S. Bedoor, W. W. Buhro, Z. Chajewski, J. M. Elson, W. G. Lynch, J. Manfredi, D. G. McNeel, W. Reviol, R. Shane, R. H. Showalter, M. B. Tsang, J. R. Winkelbauer, and A. H. Wuosmaa, *Phys. Rev. C* **92**, 034329 (2015).